

Structure of a 14-3-3 ϵ :FOXO3a^{pS253} Phosphopeptide Complex Reveals 14-3-3 Isoform-Specific Binding of Forkhead Box Class O Transcription Factor (FOXO) Phosphoproteins

Subashini Mathivanan, Puneeth Kumar Chunchagatta Lakshman, Manvi Singh, Saranya Giridharan, Keerthana Sathish, Manjunath A. Hurakadli, Kavitha Bharatham, and Neelagandan Kamariah*



Cite This: *ACS Omega* 2022, 7, 24344–24352



Read Online

ACCESS |



Metrics & More

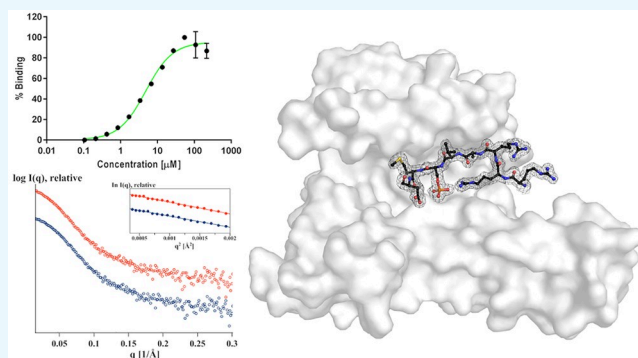


Article Recommendations



Supporting Information

ABSTRACT: The transcriptional activity of Forkhead Box O3 (FOXO3a) is inactivated by AKT-mediated phosphorylation on Serine 253 (S253), which enables FOXO3a binding to 14-3-3. Phosphorylated FOXO3a binding to 14-3-3 facilitates the nuclear exclusion of FOXO3a, causing cancer cell proliferation. The FOXO3a/14-3-3 interaction has, therefore, emerged as an important therapeutic target. Here, we report a comprehensive analysis using fluorescence polarization, isothermal titration calorimetry, small-angle X-ray scattering, X-ray crystallography, and molecular dynamics simulations to gain molecular-level insights into the interaction of FOXO3a^{pS253} phosphopeptide with 14-3-3 ϵ . A high-resolution structure of the fluorophore-labeled FOXO3a^{pS253}:14-3-3 ϵ complex revealed a distinct mode of interaction compared to other 14-3-3 phosphopeptide complexes. FOXO3a^{pS253} phosphopeptide showed significant structural difference in the positions of the -3 and -4 Arg residues relative to pSer, compared to that of a similar phosphopeptide, FOXO1^{pS256} bound to 14-3-3 σ . Moreover, molecular dynamics studies show that the significant structural changes and molecular interactions noticed in the crystal structure of FOXO3a^{pS253}:14-3-3 ϵ are preserved over the course of the simulation. Thus, this study reveals structural differences between the binding to 14-3-3 isoforms of FOXO1^{pS256} versus FOXO3a^{pS253}, providing a framework for the rational design of isoform-specific FOXO/14-3-3 protein–protein interaction inhibitors for therapy.



1. INTRODUCTION

The Forkhead box (Fox) class O transcription factor (FOXO) family contains four members: FOXO1, FOXO3a, FOXO4, and FOXO6, sharing a high homology between each other.^{1,2} Among these FOXO proteins, FOXO3a is involved in cellular apoptosis, proliferation, cell cycle progression, DNA damage, and tumorigenesis^{3,4} and is widely implicated in breast, liver, colon, prostate, bladder, and nasopharyngeal cancer.⁵ FOXO3a is a multidomain protein made up of an N-terminal DNA binding forkhead domain (FKH), nuclear localization signal (NLS), nuclear export signal (NES), and C-terminal transactivation domain (TAD) (Figure 1A). The transcriptional activity of FOXO3a is regulated by various post-translation modifications such as phosphorylation, acetylation, ubiquitination, and methylation.^{1,6} The phosphatidylinositol 3-kinase (PI3K) and protein kinase B (AKT) pathways induce phosphorylation at three key residues in FOXO3a (T24, S253, and S315), which contain an AKT consensus phosphorylation motif (RxRxxS/T, where x is any residue) in all human FOXO proteins; however, FOXO6 lacks the C-terminal phosphorylation site (corresponding to S315 of

FOXO3a) (Figure 1A).^{7,2} The S253 phosphorylation is critical for AKT-mediated nuclear exclusion of FOXO3a.^{8,9}

AKT-mediated phosphorylations enable FOXO binding to the dimeric form of the adapter protein 14-3-3 due to the overlap between the recognition motifs of AKT and 14-3-3 (RxxpS/Txp, where p is phosphate and x is any residue). This results in the translocation of FOXO from the nucleus, which subsequently inhibits the transcriptional activity of FOXO.⁷ Moreover, the basic residues in the S253 phosphorylation motif, located at the end of the DNA binding forkhead domain, are important for DNA binding activity.¹⁰ Binding of 14-3-3 to phosphorylated FOXO3a is suggested to mask the nuclear localization sequence or DNA binding site and, thereby, inactivate the FOXO3a transcription activity.^{11,12}

Received: March 21, 2022

Accepted: June 21, 2022

Published: July 5, 2022



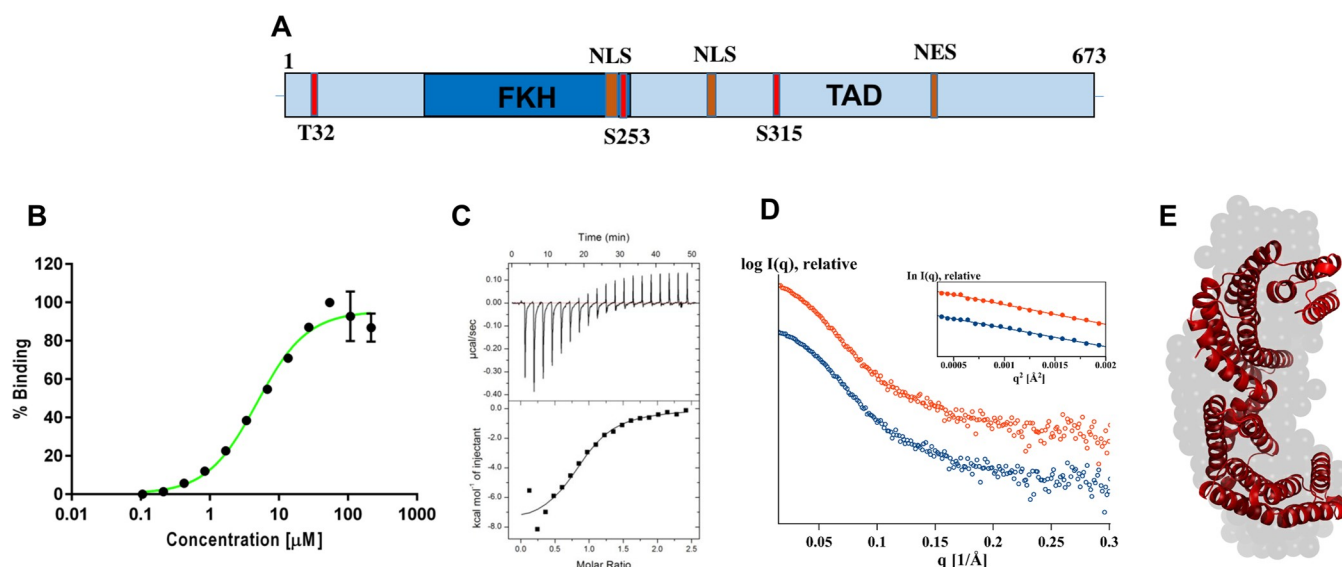


Figure 1. Phosphorylated FOXO3a^{S253} peptide bound to WT 14-3-3. (A) Schematic representation of the three distinct sites for AKT phosphorylation in FOXO3a. These phosphorylation sites likely enable FOXO3a binding to 14-3-3. Also indicated are the locations of the forkhead domain and the nuclear export (NES) and nuclear localization sequence (NLS). (B) Binding of TAMRA-labeled FOXO3a^{S253} peptide to WT 14-3-3 (monitored by FP assay). FP assay was performed in triplicate and repeated three times with similar results. Data are the mean of three independent experiments \pm SD. (C) Isothermal titration calorimetry demonstrating binding between unlabeled FOXO3a^{S253} peptide and WT 14-3-3. (A representative experiment is shown from three independent experiments.) (D) SAXS profiles with their corresponding Guinier plots (insets) are shown for WT 14-3-3 (in the absence (blue) and presence (red) of FOXO3a^{S253} phosphopeptide. For clarity, the curves are shifted by an arbitrary unit on the $I(q)$ axis. (E) Averaged ab initio model (gray sphere) overlay with the crystal structure (red cartoon, PDB ID: 2BR9).

Modulation of the FOXO/14-3-3 association is a potential anticancer strategy because FOXO is typically inactivated in human cancers by phosphorylation rather than mutation, and its reactivation inhibits cancer outgrowth.^{5,13–15}

14-3-3 proteins are a family of evolutionarily conserved modulator proteins that bind to specific Ser/Thr-phosphorylated motifs on target proteins. In humans, there are seven 14-3-3 isoforms designated by Greek letters (β , γ , ϵ , η , σ , τ , and ζ), which are known to form homo- and heterodimers.^{16,17} Each 14-3-3 protomer harbors the phosphopeptide binding groove. The seven 14-3-3 isoforms share 65–88% of sequence identity between them, but the phosphopeptide binding regions are highly conserved across the different isoforms.¹⁷ The highly conserved phosphomotif binding groove, as well as overlapping and redundant functions, made it difficult to exploit 14-3-3s for therapeutic intervention. Despite their similarities, the isoform-specific functions and isoform-specific binding to a particular phosphomotif have been established in many instances.^{18–23}

In a recent study,¹³ a biodiversity peptide library screening identified the hit peptide probe 9J10 that modulates the FOXO3a signaling pathway by interacting with the 14-3-3 protein family. The pull-down and mass spectrometry analysis revealed 14-3-3 ϵ is one among the abundant 14-3-3 proteins interacting with 9J10. Moreover, there is a sharp reduction in the interaction between 14-3-3 ϵ and FOXO3a in cells expressing the 9J10 probe signifying FOXO3a interaction with 14-3-3 ϵ . In this study, the binding of the FOXO3a^{S253} phosphopeptide motif (₂₄₈RRRAVP_{SMDNSN}₂₅₈) to 14-3-3 ϵ was measured by fluorescence polarization (FP) assay and isothermal titration calorimetry (ITC) and further structurally characterized using small-angle X-ray scattering (SAXS), X-ray crystallography, and molecular dynamics (MD) simulations. The FOXO3a^{S253}:14-3-3 ϵ complex structure solved at 1.85 Å resolution revealed a distinct structural feature compared with the highly similar FOXO1^{S256} phosphopeptide

(₂₅₁RRRAVP_{SMDNSK}₂₆₂) bound to 14-3-3 σ . This study reports the structural evidence of 14-3-3 isoform-specific binding of highly similar phosphopeptide motifs and provides a framework for the rational design of inhibitors with enhanced isoform selectivity against FOXO/14-3-3 protein–protein interactions.

2. RESULTS AND DISCUSSION

2.1. Binding of FOXO3a Phosphopeptide to 14-3-3 ϵ .

Fluorescence polarization assay was used to quantify the affinity of the tetramethylrhodamine (TAMRA)-labeled FOXO3a^{S253} phosphopeptide (TAMRA-₂₄₈RRRAVP_{SMDNSN}₂₅₈) to the wild-type (WT) 14-3-3 ϵ protein. The phosphorylated FOXO3a^{S253} peptide binds with a K_d of $5.4 \pm 0.7 \mu\text{M}$ (Figure 1B). The affinity of the unlabeled FOXO3a^{S253} phosphopeptide (₂₄₈RRRAVP_{SMDNSN}₂₅₈) to the 14-3-3 ϵ protein was measured using isothermal titration calorimetry (ITC) (Figure 1C), resulting in a comparable K_d of $6.7 \pm 1.8 \mu\text{M}$, validating no significant contribution of TAMRA on the peptide binding affinity. The calculated binding enthalpy ΔH , the K_d , the stoichiometry, n , Gibb's free energy, ΔG , and entropy, ΔS , were reported from the ITC experiment (Table S1). Our K_d determined by FP and ITC is consistent with those of previously reported 14-3-3 ϵ –phosphopeptide interactions.^{13,22}

2.2. SAXS Analysis of the 14-3-3 ϵ :FOXO3a^{S253} Complex. The SAXS patterns of WT 14-3-3 ϵ and its complex with a 6-fold molar excess of FOXO3a^{S253} phosphopeptide (TAMRA-₂₄₈RRRAVP_{SMDNSN}₂₅₈) were measured in order to determine the solution size and shape (Figure 1C). Inspection of the low angle of the Guinier plots reveals good data quality and no protein aggregation (Figure 1D, inset). 14-3-3 ϵ has a radius of gyration (R_g) of $32.23 \pm 0.37 \text{ \AA}$ and a maximum dimension (D_{max}) of $99 \pm 2 \text{ \AA}$ (Figure S1). The R_g values calculated from the real-space $P(r)$ and the Guinier

Table 1. SAXS Derived Parameters for the Full-Length 14-3-3 ϵ and the Presence of FOXO3a^{pS253} Phosphopeptide

Sample	Guinier R_g (Å)	Real space R_g (Å)	D_{max} (Å)	Calculated molecular mass (kDa) (from Porod invariant)
14-3-3 (1.6 mg/mL)	32.23 ± 0.37	32.27 ± 0.18	99 ± 2	58 ± 3
14-3-3:FOXO3a (1:6)	32.24 ± 0.41	32.25 ± 0.19	99 ± 2	58 ± 3

region resulted in similar values (Table 1). The estimated R_g , D_{max} and molecular mass of the full length indicate that 14-3-3 ϵ is dimeric at the concentrations used. The 14-3-3 ϵ contains a flexible C-terminus, which is missing in the available crystal structures, which could be the cause of the increase in the solution R_g and D_{max} values compared to those of the dimeric crystal structure of the 14-3-3 Δ C protein (R_g value of 28.9 Å and D_{max} of 85.1 Å).¹⁷ The *ab initio* solution shape of 14-3-3 ϵ was reconstructed and had a good fit to the experimental data with a discrepancy of $\chi^2 = 1$. Ten independent reconstructions produced a similar envelope with a normalized spatial discrepancy (NSD) of 1.3 ± 0.07 , and the average structure is shown in Figure 1E. The known atomic structure of 14-3-3 ϵ Δ C (PDB ID: 2BR9)¹⁷ was well positioned inside the low-resolution solution model, demonstrating a match between the solution and crystal structure. The SAXS derived parameters R_g , D_{max} and molecular mass of 14-3-3 ϵ mixed with a 1:6 molar ratio of FOXO3a^{pS253} reveal no significant oligomerization and conformational changes in 14-3-3 ϵ upon addition of the phosphopeptide (Table 1).

2.3. Overall Structure of the 14-3-3 ϵ and FOXO3a^{pS253} Phosphopeptide Complex. The crystal of TAMRA-labeled FOXO3a^{pS253} phosphopeptide bound to 14-3-3 ϵ Δ C (aa 1-232) diffracted up to 1.85 Å resolution and belongs to the C222₁ space group. The complex structure was solved, and the model was built and refined to a final R_{factor} and R_{free} of 16.55% and 18.88%, respectively. The data collection, processing, and refinement statistics are given in Table 2. The asymmetric unit contains one monomer, and the biological dimer of 14-3-3 ϵ is formed with a symmetry-related molecule generated by the crystallographic 2-fold axis. Dimeric 14-3-3 ϵ displays the characteristic W-like shape with each of the monomers harboring one FOXO3a^{pS253} phosphopeptide (Figure 2A). We found an interpretable electron density for 231 residues of 14-3-3 ϵ and 8 out of 11 residues of FOXO3a^{pS253} phosphopeptide (Figure 2B). In addition, we observed a clear electron density for the TAMRA fluorophore that is attached to the N-terminus of the FOXO3a^{pS253} phosphopeptide for estimating the binding affinity of the peptide using the FP assay (Figure 2B). The monomeric 14-3-3 ϵ structure is composed of nine helices (α A- α I) with N- and C-terminal domains spanning between the α A- α F and α G- α I helices, respectively (Figure 2A). The FOXO3a^{pS253} phosphopeptide motif (₂₄₈RRRAVPserMDNSN₂₅₈) binds in the 14-3-3 ϵ canonical peptide binding groove between the N- and C-terminal domains (Figure 2A). The phosphorylated residue FOXO3a^{pS253} interacts with the conserved binding site residues Lys50, Arg57, Arg130, and Tyr131 of 14-3-3 ϵ . Additionally, salt bridge interactions were observed for FOXO3a^{R249} and FOXO3a^{D255} with Glu183 and Lys50 of 14-3-3 ϵ , respectively (Figure 2C and Table S2). The main chain atoms of FOXO3a^{V252} and FOXO3a^{M254} are stabilized by hydrogen bonded interactions with Asn227 and Asn176, Lys50 of 14-3-3 ϵ , respectively (Table S1). However, the hydrophobic side chains of FOXO3a^{V252} and FOXO3a^{M254} are surrounded by the hydrophobic residues Leu230, Leu175, Leu223, Ile220, and Leu219 (Figure 2D). Interestingly, the FOXO3a^{R249} side

Table 2. Data Collection and Refinement Statistics of the 14-3-3 ϵ :FOXO3a^{pS253} Complex Structure^a

Parameters	14-3-3 ϵ :FOXO3a
Wavelength (Å)	0.97947
Space group	C222 ₁
Unit cell parameters	
<i>a</i> , <i>b</i> , <i>c</i> (Å)	77.88, 81.04, 83.28
α , β , γ (deg)	90 90 90
Resolution (Å)	36.44–1.85 (1.95–1.85)
R_{merge} (%)	12.0 (74.3)
Mean [$\langle I \rangle / \sigma(\langle I \rangle)$]	9.8 (2.6)
CC (1/2) (%)	99.4 (77.3)
Total no. of reflections	139,586 (18,464)
Unique reflections	22,570 (3185)
Completeness (%)	99.4 (98.1)
Multiplicity	6.2 (5.8)
Molecules in asymmetric unit	1
Solvent content (%)	47.61
Refinement statistics	
Resolution (Å)	36.44–1.85 (1.95–1.85)
R_{work} (%)	16.65 (25.7)
R_{free} (%)	18.88 (26.4)
Mean B-value (Å ²)	24.09
Ramachandran favored (%)	95.5
Ramachandran allowed (%)	4.5
Ramachandran outlier (%)	0
rms deviations	
Bond length (Å)	0.013
Bond angle (deg)	1.750

^aValues in parentheses correspond to the highest resolution shell.

chain is pointed toward FOXO3a^{pS253} and makes an intra-molecular salt bridge interaction (Figure 2D). The TAMRA moiety of the FOXO3a^{pS253} peptide does not make any significant interaction with its 14-3-3 ϵ or FOXO3a^{pS253} peptide residues in the asymmetric unit. It instead makes extensive interactions with TAMRA, Gln68 of 14-3-3 ϵ , and the FOXO3a^{R248} moiety from the neighboring symmetry-related molecule in the crystal lattice (Figure S2). However, the SAXS studies demonstrated that the TAMRA-labeled FOXO3a peptide does not affect the overall conformation and the oligomerization of 14-3-3 ϵ in solution, thus precluding any TAMRA induced artifacts (Table 1).

2.4. Structural Differences between the FOXO3a^{pS253}:14-3-3 ϵ and FOXO1^{pS253}:14-3-3 σ Complexes.

Three distinct phosphopeptide binding motifs for 14-3-3 have been identified and defined as mode 1 (RSxpS/T-xP; PDB ID: 1QJB), mode 2 (RxxxpS/T-xP; PDB ID: 1QJA) and mode 3 (pS/pTX₁₋₂-COOH), wherein pS and pT are phosphorylated Ser and Thr, respectively, and X is any amino acid.^{24,25} In mode I and mode 2, proline is preferred at position +2 with respect to the pSer or pThr, and arginine, at −3 and −4 in mode 1 and mode 2, respectively. In mode III, the pSer or pThr is the penultimate residue in the C-terminal tail of a binding partner. In addition, the recently solved structure of FOXO1^{pS256} bound 14-3-3 σ (₂₅₂RRRAApSMD₂₅₈; PDB ID:

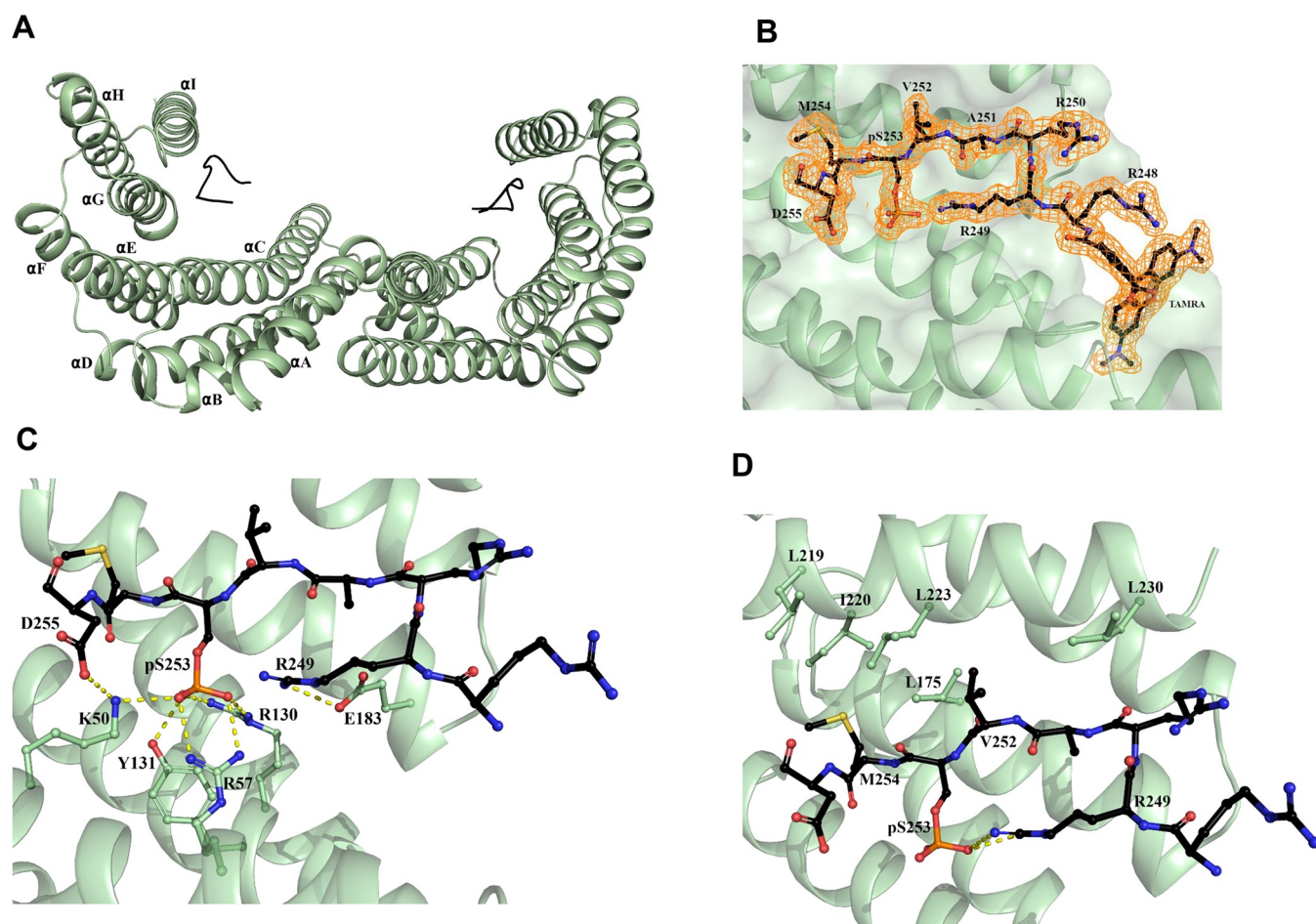


Figure 2. Cocystal structure of FOXO3a^{pS253} peptide and 14-3-3 ϵ Δ C. (A) Ribbon representation of the 14-3-3 ϵ dimer with each monomer (green cartoon) binding a FOXO3a^{pS253} phosphopeptide (black stick). (B) 2Fo-Fc map contour at the 1 σ level around the FOXO3a^{pS253} peptide residues (orange mesh), from the cocystal structure. The map clearly shows the FOXO3a peptide region. (C) Phosphate moiety of FOXO3a^{pS253} (black stick) anchored on the conserved Tyr131, Arg130, Arg57, and Lys50 residues of 14-3-3 ϵ (green stick). Salt bridge interactions were observed for FOXO3a^{Arg249} and FOXO3a^{Asp255} with Glu183 and Lys50 of 14-3-3 ϵ , respectively. (D) 14-3-3 ϵ residues creating a hydrophobic environment for FOXO3a^{V252} and FOXO3a^{M254}. The unique intramolecular interaction of FOXO3a^{R249} with FOXO3a^{pS253} is shown.

6QZS),²⁶ which is highly similar to FOXO3a^{pS253}, was available for structural comparison. In the FOXO1^{pS256}:14-3-3 σ complex structure, the residues from Arg²⁵² to Asp²⁵⁸ spanning from the -4 to +2 positions relative to pSer are built into the electron density out of the 12 amino acids of the FOXO1^{pS256} peptide (²⁵¹RRRAApSMDNNSK²⁶²). Here in the FOXO3a^{pS253}:14-3-3 ϵ structure, the residues from Arg²⁴⁸ to Asp²⁵⁵ spanning from the -5 to +2 positions relative to pSer are built into the electron density from the 11 amino acid FOXO3a^{pS253} peptide (₂₄₈RRRAVpSerMDNSN₂₅₈). Therefore, the 14-3-3 binding motifs in both the FOXO3a^{pS253} and FOXO1^{pS256} peptides are highly similar in length and sequence, except there is one amino acid where FOXO3a^{V252} is replaced by FOXO1^{A255} at the -1 position relative to pSer. The FOXO3a^{pS253} and FOXO1^{pS256} motifs are not positioned at the C-terminus of the full-length proteins and have the canonical binding sequence (RRRAV/ApSMD), thereby representing either mode 1 or 2 in this case. The mode 1 and mode 2 motifs have invariant Pro at the +2 position with respect to pSer, while FOXO3a/FOXO1 has negatively charged Asp at the +2 position with respect to pSer. The presence of a Pro at the +2 position is known to introduce a kink in the mode 1 and 2 motifs, which leads the peptide chain to exit the central binding channel and cross the 14-3-3 monomer in the direction of the adjacent

monomer (Figure 3A and B). Interestingly, the FOXO3a/FOXO1 phosphopeptide Asp at the +2 position makes the kink, which enables the peptide chain to exit from the binding groove and is more similar to that of the mode 2 peptide motif than the mode 1 motif (Figure 3). A significant difference is observed in the side chain conformation +2 Asp between the FOXO3a^{pS253} and FOXO1^{pS256} motifs. The negatively charged carboxylic acid group of the +2 Asp is pulled toward the positively charged phosphopeptide binding pocket, makes a salt bridge interaction with the phosphopeptide binding residue, Lys50, and is the cause for the kink to exit the central binding channel in the FOXO3a^{pS253} peptide (Figure 3C). In contrast, the +2 Asp is pointed outward and solvent-exposed in the FOXO1^{pS256} peptide (Figure 3C). Another interesting feature in the FOXO3a^{pS253} peptide structure is the salt bridge interaction between the pSer phosphate oxyanion and Lys50, which is a highly conserved residue across the different isoforms of 14-3-3. Lys50 interacts with the pSer phosphate oxyanion in the mode 1 and mode 2 motifs, but this interaction is missing in the so far known structures of 14-3-3 ϵ and FOXO1 (Figure S2). The Lys50 side chain is either disordered (PDB ID: 2BR9)¹⁷ or oriented outward (PDB ID: 6EIH)²⁷ or occluded (PDB ID: 3UAL)²² to prevent the interaction with the pSer phosphate oxyanion (Figure S3). However, the

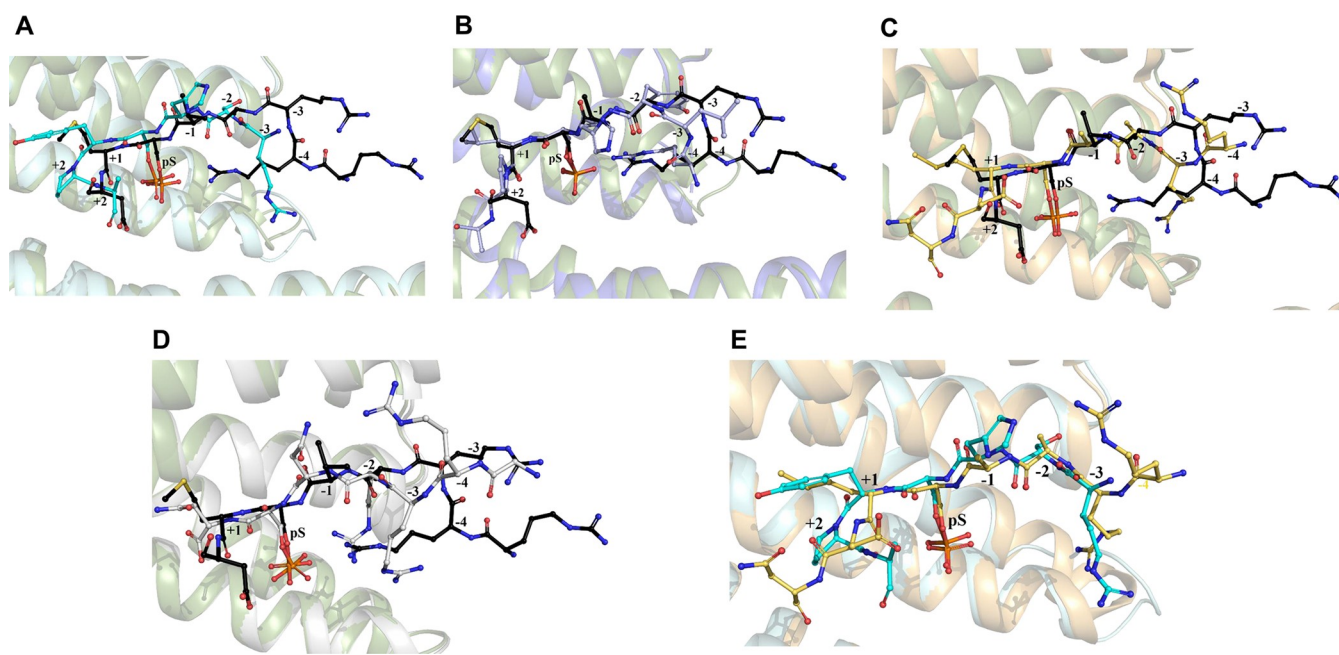


Figure 3. Comparison of the FOXO3a^{pS253} binding mode with other 14-3-3 binding motifs. The 14-3-3 protein is shown as a cartoon representation, and the bound phosphopeptides are shown as stick representations. The bound phosphopeptide residue position with respect to pSer is highlighted. Structural overlay of 14-3-3 bound FOXO3a^{pS253} (black sticks) with the (A) mode 1 peptide (cyan sticks, PDB ID: 1QJB), (B) mode 2 peptide (light blue sticks, PDB ID: 1QJA), (C) FOXO1^{pS256} peptide (yellow sticks, PDB ID: 6QZS), and (D) 9J10 peptide (gray sticks, PDB ID: 7C8E). (E) Structural overlay of the FOXO1^{pS256} peptide (yellow stick, PDB ID: 6QZS) with the mode 1 peptide (cyan stick, PDB ID: 1QJB).

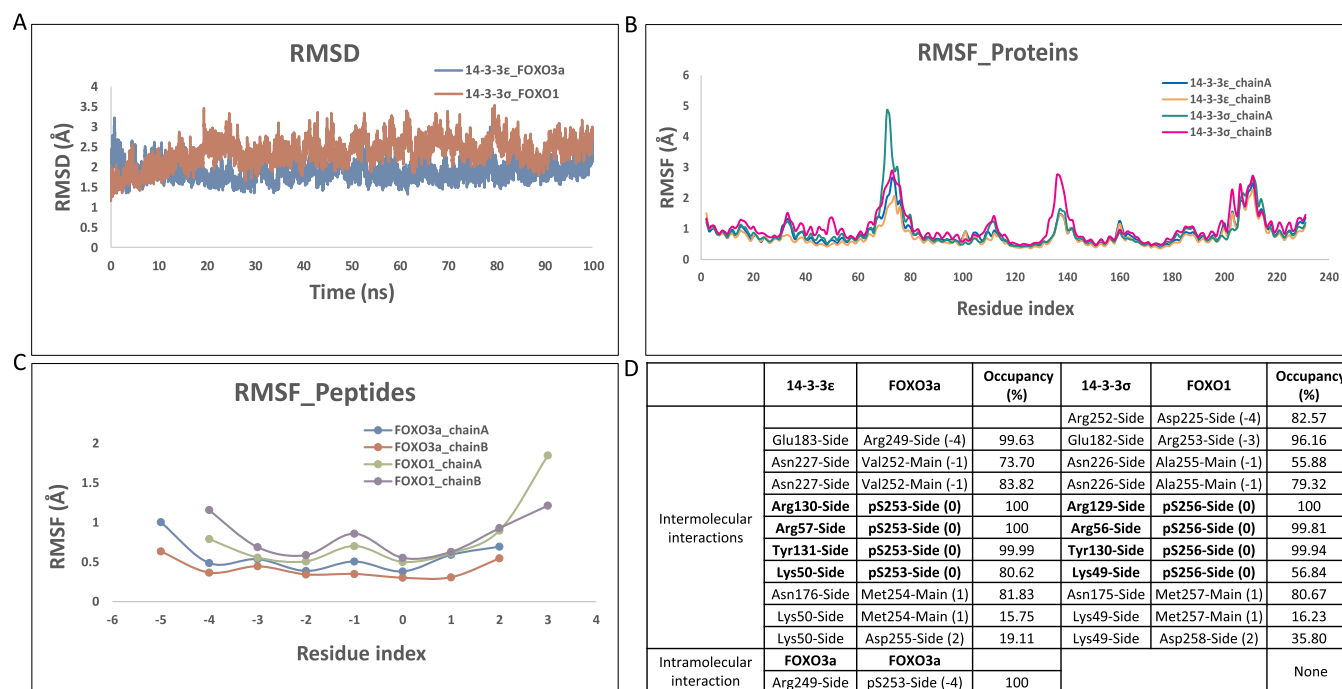


Figure 4. MD simulation analyses of the FOXO3a^{pS253}:14-3-3ε and FOXO1^{pS256}:14-3-3σ complexes during a 100 ns simulation. (A) RMSD of the 14-3-3ε:FOXO3a^{pS253} protein backbone atoms (blue) and 14-3-3σ: FOXO1^{pS256} (red) with respect to their respective initial reference frame. (B) RMSF of the 14-3-3ε and 14-3-3σ protein chains (the residue index is shown for 14-3-3ε). (C) RMSF of the FOXO3a^{pS253} and FOXO1^{pS256} phosphopeptide chains. (D) H-bond occupancy of intra- and intermolecular interacting residue pairs of the FOXO3a^{pS253}:14-3-3ε and FOXO1^{pS256}:14-3-3σ complexes. The peptide residue index is shown in the parentheses.

carboxylic acid group of Asp +2 stabilizes the Lys50 position similar to the mode 1 and mode 2 motifs and preserves the Lys50 interaction with the phosphopeptide motif. Moreover, a subtle difference is observed in the side chain conformation of

the +1 Met position between the FOXO3a^{pS253} and FOXO1^{pS256} peptides (Figure 3C). The FOXO3a Met side chain is well surrounded by the hydrophobic residues Gly172, Leu175, Ile220, and Leu223.

A second interesting aspect of the FOXO3a/FOXO1 phosphopeptide is the position of arginines, as both the phosphopeptides contain consecutive Arg's at the -3 , -4 , and -5 positions with respect to pSer, whereas the mode 1 and mode 2 peptides have Arg at either -3 or -4 with respect to pSer and have been demonstrated to be critical for binding.²⁸ In the mode 1 structure, -3 Arg enables a kink in the phosphopeptide to exit the central pocket in the direction of the adjacent 14-3-3 monomer, but there is no clear electron density to locate its side chain (Figure 3A). Similarly, -3 Arg introduces a kink in the FOXO1 peptide to exit the central binding groove while the peptide chain returns into the pocket at -4 Arg and there is no clear side chain electron density for both Arg's at the -3 and -4 positions with respect to pSer (Figure 3C and E).²⁶ In contrast, in the mode 2 peptide, a large kink is introduced by -4 Arg, and its side chain folds back to point toward the pSer forming an intramolecular salt bridge between the guanidine group of Arg and the pSer phosphate oxyanion (Figure 3B). In the FOXO3a phosphopeptide, the backbone positions of the -3 and -4 Arg residues of FOXO3a are significantly different compared to those from the mode 1, mode 2, and FOXO1 peptides (Figure 3A–C). The difference is mainly due to the fact that the mode 2 peptide has the aromatic residue Tyr at the pSer -2 position (₃RLYHpSLPA₁₀) instead of Ala at pSer -2 in FOXO3a^{pS253}. The side chain of -2 Tyr occupies the central binding groove, and -3 Arg exits the central binding groove (Figure 3B). However, the FOXO3a -3 Arg continues to lie in the central binding groove, and only -4 Arg makes a large kink and its side chain points toward the pSer to form an intramolecular interaction.

In both the mode 2 and FOXO3a structures, the -4 Arg guanidino group is located at the same position, and Arg is further stabilized by an additional salt bridge between the δ NH of the arginine guanidino group and the carboxyl side chain of the highly conserved Glu180 (Figure 3B). We observed a similar intramolecular interaction between -2 Arg and the pSer of 9J10 phosphopeptide (LNTRPGRRRNpSN) in our recently reported structure (Figure 3D; PDB ID: 7C8E).¹³ These results show that Arg at the -2 , -3 , or -4 position brings significant structural differences in the binding mode of phosphopeptides.

2.5. MD Simulation Studies of FOXO3a^{pS253}:14-3-3 ϵ and FOXO1^{pS256}:14-3-3 σ Complexes. To comprehend the distinct binding modes of FOXO phosphopeptides in the binding channel of the 14-3-3 substrate, explicit solvent MD simulations lasting 100 ns were performed for the complexes. The RMSD (root mean square deviations) of the backbone atoms of the FOXO3a^{pS253}:14-3-3 ϵ (PDB ID: 7V9B) and FOXO1^{pS256}:14-3-3 σ (PDB ID: 6QZS) complexes were stabilized at 2 and 2.5 Å compared to their respective cocrystal structures (Figure 4A), suggesting that the simulations were stable. The C α atom RMSF (root mean square fluctuation) calculations indicate that 14-3-3 is stable with noticeable changes in loop regions 71–76 and 206–215 for 14-3-3 ϵ and 74–82, 140–144, and 211–220 for 14-3-3 σ (Figure 4B). The C α atom RMSF calculations of the phosphopeptides show that the $+1$ to -4 residues relative to pSer of the FOXO3a and FOXO1 phosphopeptides are stable with ~ 0.5 Å and ~ 0.6 Å RMSF, respectively, with the FOXO3a -1 position residue, Val252 being more stable than the corresponding residue Ala255 in FOXO1 (Figure 4C). Further, the occupancy analysis of the H-bonds as summarized in Figure 4D shows

that the phosphorylated residue FOXO3a^{pS253} makes an H-bond interaction with the conserved binding pocket residues Lys50, Arg57, Arg130, and Tyr131 of 14-3-3 ϵ with 80.6%, 100%, 100%, and 100% occupancy. Similar interactions were observed between FOXO1^{pS256} and 14-3-3 σ .

The main chain of FOXO3a^{M254} makes an H-bond interaction with Asn176 and Lys50 of 14-3-3 ϵ , with 81.8% and 15.7% occupancy, respectively (Figure 4D), while the side chain is surrounded by hydrophobic residues, Gly172, Leu175, Ile220, and Leu223 of 14-3-3 ϵ . A similar interaction pattern was observed with FOXO1^{M257}. The distinctive residues at the -1 position relative to pSer, FOXO3a^{V252} and FOXO1^{A255}, make two main chain H-bond interactions each with the 14-3-3 ϵ Asn227 and 14-3-3 σ Asn226 side chains, respectively. The stable H-bond interactions made by the FOXO3a^{Val252} main chain are likely due to the additional hydrophobic interaction made by its side chain with 14-3-3 ϵ Leu175, Leu223, and Leu230, unlike the case of FOXO1^{Ala255}. FOXO3a^{R248} (-3 R position relative to pSer) is solvent exposed while the FOXO1^{R253} (-3 R position relative to pSer) guanidine group interacts with Glu182 side chain with 96.2% occupancy. FOXO3a^{R249} (-4 R position relative to pSer) forms an intramolecular salt bridge interaction with FOXO3a^{pS253} while engaging Glu183 of 14-3-3 ϵ with occupancies of 100% and 99.6%, unlike FOXO1^{R252} (-4 R position relative to pSer), which interacts with the Asp225 side chain with 82.6% occupancy (Figure 4D). Overall, MD simulation studies support the structural changes noticed at the -3 and -4 Arg residues in the phosphopeptide binding mode between the two FOXO3a^{pS253}:14-3-3 ϵ and FOXO1^{pS256}:14-3-3 σ cocrystal structures.

3. CONCLUSIONS

In summary, we have characterized the binding mechanism of the FOXO3a^{pS253} phosphopeptide to 14-3-3 ϵ using FP, ITC, SAXS, X-ray crystallography, and MD simulation studies. The cocrystal structure demonstrated that the TAMRA-labeled FOXO3a^{pS253} phosphopeptide binds to 14-3-3 ϵ in a distinct manner compared to that of the highly homologous FOXO1^{pS256} peptide binding to 14-3-3 σ . Further, the FOXO3a and FOXO1 phosphopeptides resemble the mode 2 and mode 1 peptide motifs for binding to 14-3-3, respectively. Though closely resembling mode 2, FOXO3a showed a significant difference in the backbone positions of the -3 and -4 Arg residues compared to those from a canonical mode 2 peptide. Moreover, MD simulation studies confirmed that the structural changes noticed in the crystal structure of FOXO3a^{pS253}:14-3-3 ϵ and the observed molecular interactions are preserved over the course of the simulation. Together, our data illustrate that the highly similar FOXO phosphopeptides adopt a distinct binding interaction with the conserved phosphomotif binding groove in 14-3-3s. Previous studies strongly support the notion of the 14-3-3 isoform-specific binding of phosphopeptide.^{18–23} Interestingly, a recent study suggests the hierarchized profile in binding affinities of 14-3-3 isoforms to the phosphopeptide.²⁹ Probing the FOXO3a–14-3-3 interaction has potential therapeutic significance because FOXO3a is frequently inactivated in many cancers by Akt-mediated phosphorylation and subsequent 14-3-3 binding.^{5,30} The observed isoform-specific binding lays the groundwork for developing protein–protein interaction inhibitors with enhanced isoform selectivity against FOXO:14-3-3 complexes.

4. MATERIALS AND METHODS

4.1. Cloning, Expression, and Purification. The WT 14-3-3 ϵ and 14-3-3 $\epsilon\Delta$ C (aa 1-232) genes were PCR amplified and then inserted into the pET28a vector (Novagen 69864-3) containing an N-terminal 6xHis tag with a thrombin cleavage site, using the *Bam*HI and *Xho*I restriction enzyme sites. The plasmid was later expressed in *E. coli* BL21 DE3 cells. The culture was grown in Luria broth media containing kanamycin (50 μ g/mL) at 37 °C. The cells were induced with 1 mM isopropyl β -D-1-thiogalactopyranoside (IPTG) once the O.D.600 nm reached 0.6 and continuously grown for 4 h at 37 °C. The cells were harvested by centrifugation and resuspended in the buffer containing 50 mM Tris pH 7.5, 300 mM NaCl, 1 mM DTT, 0.1 mM PMSF, and 1 protease inhibitor tablet followed by lysis by sonication. The lysate was centrifuged, and the supernatant was passed through a 5 mL Ni-NTA IMAC column, followed by washes with 50 mM Tris pH 7.5, 300 mM NaCl, 1 mM DTT, and 0–20 mM imidazole. The bound protein was eluted using 50 mM Tris pH 7.5, 300 mM NaCl, 1 mM DTT, and 500 mM imidazole. The affinity purified protein was then injected into a S75 Superdex size exclusion column. For crystallization, the 14-3-3 $\epsilon\Delta$ C protein was subjected to thrombin digestion to remove the 6xHis-tag prior to purifying using a size exclusion column.

4.2. Fluorescence Polarization (FP). FP assay was performed using black 96 well plates (LVL Technologies). In direct binding FP experiments, 15 nM TAMRA-conjugated synthetic FOXO3a^{pS253} phosphopeptide (Designer Bioscience Ltd., UK) was mixed with increasing concentrations of WT 14-3-3 ϵ protein (from 0.002 μ M to 63 μ M) in triplicate. The assay volume was 30 μ L per reaction with 3 \times working concentrations of protein and peptide, 10 μ L each prepared in assay buffer (10 mM HEPES pH 7.5, 150 mM NaCl, 0.5 mM DTT, and 0.005% Tween 20). The plate was incubated for 10 min at room temperature, and relative fluorescence was measured with the excitation wavelength of 530 nm and an emission wavelength of 610 nm using the TECAN infinite M1000 Pro microplate reader (TECAN). The degree of polarization ratio of fluorescence intensities parallel and perpendicular was calculated by the reader using iControl software and expressed in millipolarization units (mP). The FP values were plotted against the log of the 14-3-3 ϵ protein concentrations, and the binding affinity, K_d was determined from the generated sigmoidal curve as analyzed in GraphPad Prism 6.

4.3. Isothermal Titration Calorimetry. Wild-type 14-3-3 ϵ was dialyzed in a buffer containing 20 mM HEPES, pH 7.5, 150 mM NaCl, and 1 mM DTT. Unlabeled FOXO3a^{pS253} phosphopeptide (GaloreTx Pharmaceuticals Pvt. Ltd., India) was dissolved in the same buffer as mentioned above. ITC experiments were performed using MicroCal ITC 200 at 25 °C in high-feedback mode with stirring speed 800 rpm and filter period time 5 s. 50 μ M FOXO3a^{pS253} phosphopeptide was titrated with 20 injections of 590 μ M WT 14-3-3 ϵ , with each 2 μ L injection with a 150 s interval between each injection. A control experiment was conducted with identical buffer conditions and peptide in the cell replaced by buffer, and this control experimental result was used to subtract to account for the heat of dilution. The data was analyzed by origin 7 software, and the results were fit by using a one set of sites model.

4.4. SAXS Data Collection and Analysis. SAXS data of WT 14-3-3 ϵ were measured at 1.6 mg/mL in a buffer containing 50 mM Tris/HCl, pH 7.5, and 200 mM NaCl using a BIOSAXS-1000 Rigaku instrument with a microfocus X-ray generator (1.5418 Å wavelength). The measurement with FOXO3a phosphopeptide was performed with a 6-fold excess of the peptide. For each protein sample, data were collected for a corresponding buffer under identical experimental conditions, providing a background scattering to subtract from the scattering of the sample. All the data processing steps were performed using PRIMUS.³¹ The low- q region of the Guinier plot was used to analyze for protein aggregation. The forward scattering $I(0)$ and the radius of gyration, R_g , were computed using the Guinier approximation assuming that at very small angles ($q < 1.3/R_g$) the intensity is represented as $I(q) = I(0) \exp(-(qR_g)^2/3)$. The distance distribution function $P(r)$ of the maximum particle dimension, D_{max} and the radius of gyration, R_g , were also computed from the extended scattering patterns using the indirect transform package GNOM.³² GASBOR³³ was used to build ab initio low-resolution models considering low angle data ($q < 2 \text{ nm}^{-1}$). The ab initio solution shape was obtained by superposition of 10 independent model reconstructions with the program SUPCOMB³⁴ and then averaged using DAMAVER.³⁵ The ab initio model was superposed with the X-ray structure using SUPCOMB.

4.5. Crystallization and Structure Determination. The purified, 5 mg/mL 14-3-3 $\epsilon\Delta$ C protein was incubated with the FOXO3a^{pS253} peptide (TAMRA-RRRAVP SMDNSN) at a ratio of 1:1 (0.15 mM:0.15 mM) supplemented with 20 mM HEPES, pH 7.5, 0.05 mM EDTA, and 1 mM MgCl₂. The protein mixture was screened using Hampton and Jena Bioscience (Basic and Classic) condition kits using sitting drop at 16 °C. Diffracting quality crystals were later obtained using the hanging drop vapor diffusion method at 16 °C, in conditions containing 30% MPD, 10% PEG 4000, 0.1 M imidazole HCl, pH 8.0. These crystals were flash frozen in liquid nitrogen and shipped to the PXBL-21 beamline of the Indus-2 synchrotron facility (RRCAT, Indore, India).³⁶ The diffraction data were collected up to 1.85 Å at 100 K using an X-ray beam with a wavelength of 0.97 Å and a MARCCD 225 mm detector. The diffraction images were processed and integrated using iMOSFLM³⁷ and later scaled using the Scala program³⁸ (Evans, 2006) in the CCP4 suite.^{39,40} The initial structure solution of the protein was obtained by the MR method using the Phaser MR module,⁴¹ with the monomer unit of 14-3-3 $\epsilon\Delta$ C as the starting model (PDB ID: 2BR9).¹⁷ Further model building was done in Coot⁴² followed by refinement using the REFMAC5 program.⁴³ The atomic coordinate and structure factor have been deposited in the RCSB PDB with accession code 7V9B.

4.6. Molecular Dynamics (MD) Simulations. MD simulations lasting 100 ns were performed for complexes using the Amber99SB force field of the Amber18 package.⁴⁴ Hydrogens were added, and the protonation state of ionizable groups was chosen to pH 7.0. Missing residues were added, and the terminal residues were patched with acetyl at the N-terminal and an N-methyl group at the C-terminal of the peptide and protein, as they were not the natural termini. The parameters for pSer were obtained as described in ref 45. Energy minimization and MD simulations were carried out with PMEMD MD. Minimization was performed by the steepest descent method for the first 3000 steps followed by 2000 steps of the conjugated gradient method. First, the two

peptides within the complex were minimized with the restraints of a harmonic force constant of 100.0 kcal/(mol·Å²) applied to all protein heavy atoms. The protein and peptide were then minimized with no restraints. Each minimized complex was inserted in a water box of TIP3P water that extended 10 Å from the complex and neutralized by adding counterions. Water molecules alone were minimized while restraining all protein and peptide heavy atoms. Finally, all restraints were removed, and the total system (protein, peptide, and solvent) was minimized. After energy minimization, the system was slowly heated from 0 to 300.0 K over 100 ps in the NPT ensemble under 1 atm of pressure. Equilibration was done in three steps of 100 ps each starting with 10.0 kcal/(mol·Å²) harmonic restraint weight followed by 1.0 kcal/(mol·Å²) on all heavy atoms and ending with a final equilibration with no restraints. Production runs of 100 ns were carried out without any restraint at a temperature of 300.0 K and a pressure of 1 atm using a time step of 2 fs. A 12.0 Å cutoff was used as nonbonded cutoff, and bond lengths involving bonds to hydrogen atoms were constrained using the SHAKE algorithm.⁴⁶ The coordinates were stored every 20 ps. RMSD/RMSF was measured by utilizing the Amber analyses tool PTRAJ. The hydrogen-bonding analysis tool incorporated in the VMD software⁴⁷ was utilized to calculate the hydrogen bond interaction analyses of the MD trajectories.

■ ASSOCIATED CONTENT

SI Supporting Information

The Supporting Information is available free of charge at <https://pubs.acs.org/doi/10.1021/acsomega.2c01700>.

Pair-distance distribution function $P(r)$ for 14-3-3 ϵ in the absence and presence of the FOXO3a^{S253} peptide (Figure S1); TAMRA-mediated interactions between the FOXO3a^{S253} peptide and 14-3-3 ϵ (Figure S2); comparison of Lys50 of the 14-3-3 ϵ interaction with pSer (Figure S3); ITC thermodynamic values of the 14-3-3 ϵ and FOXO3a^{S253} peptide interaction (Table S1); interactions between the 14-3-3 ϵ and FOXO3a^{S253} peptide (Table S2) (PDF)

■ AUTHOR INFORMATION

Corresponding Author

Neelagandan Kamariah – Centre for Chemical Biology & Therapeutics, inStem & NCBS, Bangalore 560065, India;
orcid.org/0000-0002-7511-7161;
Email: neelagandank@instem.res.in

Authors

Subashini Mathivanan – Centre for Chemical Biology & Therapeutics, inStem & NCBS, Bangalore 560065, India
Puneeth Kumar Chunchagatta Lakshman – Centre for Chemical Biology & Therapeutics, inStem & NCBS, Bangalore 560065, India
Manvi Singh – Centre for Chemical Biology & Therapeutics, inStem & NCBS, Bangalore 560065, India
Saranya Giridharan – Centre for Chemical Biology & Therapeutics, inStem & NCBS, Bangalore 560065, India
Keerthana Sathish – Centre for Chemical Biology & Therapeutics, inStem & NCBS, Bangalore 560065, India;
orcid.org/0000-0002-2773-7489
Manjunath A. Hurakadli – Centre for Chemical Biology & Therapeutics, inStem & NCBS, Bangalore 560065, India

Kavitha Bharatham – Centre for Chemical Biology & Therapeutics, inStem & NCBS, Bangalore 560065, India

Complete contact information is available at:
<https://pubs.acs.org/doi/10.1021/acsomega.2c01700>

Author Contributions

S.M. determined and analyzed structure of the FOXO3a/14-3-3 complex. P.C. and K.S. performed SAXS. S.G. performed the FP assay. M.A.H. performed the ITC. M.S. and K.B. carried out the molecular dynamics simulations. K.N. designed the experiments, supervised, and analyzed the FP, ITC, SAXS, and crystallography data. K.N. wrote the paper with assistance from the other authors.

Notes

The authors declare no competing financial interest.

■ ACKNOWLEDGMENTS

This work was funded by Department of Biotechnology, Government of India, reference no. BT/PR7222/MED/31/1901/2012. We thank the staff of beamline PXBL-21 at the Indus-2 Synchrotron facility (RRCAT, Indore, India) for expert help with data collection.

■ REFERENCES

- (1) Calnan, D.; Brunet, A. The foxo code. *Oncogene* **2008**, *27* (16), 2276–2288.
- (2) Tzivion, G.; Dobson, M.; Ramakrishnan, G. FoxO transcription factors; Regulation by AKT and 14–3-3 proteins. *Biochimica et Biophysica Acta (BBA)-Molecular Cell Research* **2011**, *1813* (11), 1938–1945.
- (3) Ho, Y.; Myatt, S.; Lam, E. W. Many forks in the path: cycling with FoxO. *Oncogene* **2008**, *27* (16), 2300–2311.
- (4) Nho, R. S.; Hergert, P. FoxO3a and disease progression. *World journal of biological chemistry* **2014**, *5* (3), 346.
- (5) Liu, Y.; Ao, X.; Ding, W.; Ponnusamy, M.; Wu, W.; Hao, X.; Yu, W.; Wang, Y.; Li, P.; Wang, J. Critical role of FOXO3a in carcinogenesis. *Molecular Cancer* **2018**, *17* (1), 1–12.
- (6) Daitoku, H.; Sakamaki, J.-i.; Fukamizu, A. Regulation of FoxO transcription factors by acetylation and protein-protein interactions. *Biochimica et Biophysica Acta (BBA)-Molecular Cell Research* **2011**, *1813* (11), 1954–1960.
- (7) Brunet, A.; Bonni, A.; Zigmond, M. J.; Lin, M. Z.; Juo, P.; Hu, L. S.; Anderson, M. J.; Arden, K. C.; Blenis, J.; Greenberg, M. E. Akt promotes cell survival by phosphorylating and inhibiting a Forkhead transcription factor. *cell* **1999**, *96* (6), 857–868.
- (8) Nakae, J.; Barr, V.; Accili, D. Differential regulation of gene expression by insulin and IGF-1 receptors correlates with phosphorylation of a single amino acid residue in the forkhead transcription factor FKHR. *EMBO journal* **2000**, *19* (5), 989–996.
- (9) Zhang, X.; Gan, L.; Pan, H.; Guo, S.; He, X.; Olson, S. T.; Mesecar, A.; Adam, S.; Unterman, T. G. Phosphorylation of serine 256 suppresses transactivation by FKHR (FOXO1) by multiple mechanisms: direct and indirect effects on nuclear/cytoplasmic shuttling and DNA binding. *J. Biol. Chem.* **2002**, *277* (47), 45276–45284.
- (10) Tsai, K.-L.; Sun, Y.-J.; Huang, C.-Y.; Yang, J.-Y.; Hung, M.-C.; Hsiao, C.-D. Crystal structure of the human FOXO3a-DBD/DNA complex suggests the effects of post-translational modification. *Nucleic acids research* **2007**, *35* (20), 6984–6994.
- (11) Obsil, T.; Obsilova, V. Structural basis for DNA recognition by FOXO proteins. *Biochimica et Biophysica Acta (BBA)-Molecular Cell Research* **2011**, *1813* (11), 1946–1953.
- (12) Silhan, J.; Vacha, P.; Strnadova, P.; Vecer, J.; Herman, P.; Sulc, M.; Teisinger, J.; Obsilova, V.; Obsil, T. 14–3-3 protein masks the DNA binding interface of forkhead transcription factor FOXO4. *J. Biol. Chem.* **2009**, *284* (29), 19349–19360.

- (13) Emery, A.; Hardwick, B. S.; Crooks, A. T.; Milech, N.; Watt, P. M.; Mithra, C.; Kumar, V.; Giridharan, S.; Sadasivam, G.; Mathivanan, S. Target identification for small-molecule discovery in the FOXO3a tumor-suppressor pathway using a biodiverse peptide library. *Cell Chemical Biology* **2021**, *28* (11), 1602–1615.
- (14) Farhan, M.; Wang, H.; Gaur, U.; Little, P. J.; Xu, J.; Zheng, W. FOXO signaling pathways as therapeutic targets in cancer. *International journal of biological sciences* **2017**, *13* (7), 815.
- (15) Yang, J.-Y.; Hung, M.-C. A new fork for clinical application: targeting forkhead transcription factors in cancer. *Clinical cancer research* **2009**, *15* (3), 752–757.
- (16) Fu, H.; Subramanian, R. R.; Masters, S. C. 14–3-3 proteins: structure, function, and regulation. *Annual review of pharmacology and toxicology* **2000**, *40* (1), 617–647.
- (17) Yang, X.; Lee, W. H.; Sobott, F.; Papagrigoriou, E.; Robinson, C. V.; Grossmann, J. G.; Sundström, M.; Doyle, D. A.; Elkins, J. M. Structural basis for protein-protein interactions in the 14–3-3 protein family. *Proc. Natl. Acad. Sci. U. S. A.* **2006**, *103* (46), 17237–17242.
- (18) Dougherty, M. K.; Morrison, D. K. Unlocking the code of 14–3-3. *Journal of cell science* **2004**, *117* (10), 1875–1884.
- (19) Manschwetus, J. T.; Wallbott, M.; Fachinger, A.; Obergruber, C.; Pautz, S.; Bertinetti, D.; Schmidt, S. H.; Herberg, F. W. Binding of the human 14–3-3 isoforms to distinct sites in the leucine-rich repeat kinase 2. *Frontiers in Neuroscience* **2020**, *14*, 302.
- (20) Sengupta, A.; Liriano, J.; Bienkiewicz, E. A.; Miller, B. G.; Frederich, J. H. Probing the 14–3-3 Isoform-Specificity Profile of Protein-Protein Interactions Stabilized by Fusicoccin A. *ACS omega* **2020**, *5* (39), 25029–25035.
- (21) Centorrino, F.; Ballone, A.; Wolter, M.; Ottmann, C. Biophysical and structural insight into the USP8/14–3-3 interaction. *FEBS letters* **2018**, *592* (7), 1211–1220.
- (22) Molzan, M.; Weyand, M.; Rose, R.; Ottmann, C. Structural insights of the MLF1/14–3-3 interaction. *FEBS journal* **2012**, *279* (4), 563–571.
- (23) Uhart, M.; Bustos, D. M. Human 14–3-3 Paralogs Differences Uncovered by Cross-Talk of Phosphorylation and Lysine Acetylation. *PLoS One* **2013**, *8* (2), No. e55703.
- (24) Rittinger, K.; Budman, J.; Xu, J.; Volinia, S.; Cantley, L. C.; Smerdon, S. J.; Gamblin, S. J.; Yaffe, M. B. Structural analysis of 14–3-3 phosphopeptide complexes identifies a dual role for the nuclear export signal of 14–3-3 in ligand binding. *Molecular cell* **1999**, *4* (2), 153–166.
- (25) Coblitz, B.; Shikano, S.; Wu, M.; Gabelli, S. B.; Cockrell, L. M.; Spieker, M.; Hanyu, Y.; Fu, H.; Amzel, L. M.; Li, M. C-terminal recognition by 14–3-3 proteins for surface expression of membrane receptors. *J. Biol. Chem.* **2005**, *280* (43), 36263–36272.
- (26) Saline, M.; Badertscher, L.; Wolter, M.; Lau, R.; Gunnarsson, A.; Jacso, T.; Norris, T.; Ottmann, C.; Snijder, A. AMPK and AKT protein kinases hierarchically phosphorylate the N-terminus of the FOXO1 transcription factor, modulating interactions with 14–3-3 proteins. *J. Biol. Chem.* **2019**, *294* (35), 13106–13116.
- (27) Borisova, M. E.; Voigt, A.; Tollenaere, M. A.; Sahu, S. K.; Juretschke, T.; Kreim, N.; Mailand, N.; Choudhary, C.; Bekker-Jensen, S.; Akutsu, M. p38-MK2 signaling axis regulates RNA metabolism after UV-light-induced DNA damage. *Nat. Commun.* **2018**, *9*, 1017.
- (28) Yaffe, M. B.; Rittinger, K.; Volinia, S.; Caron, P. R.; Aitken, A.; Leffers, H.; Gamblin, S. J.; Smerdon, S. J.; Cantley, L. C. The structural basis for 14–3-3: phosphopeptide binding specificity. *Cell* **1997**, *91* (7), 961–971.
- (29) Gogl, G.; Tugaeva, K. V.; Eberling, P.; Kostmann, C.; Trave, G.; Sluchanko, N. Hierarchized phosphotarget binding by the seven human 14–3-3 isoforms. *Nature Communication* **2021**, *12*, 1677.
- (30) Hornsveld, M.; Dansen, T. B.; Derksen, P. W.; Burgering, B. M. T. Re-evaluating the role of FOXOs in cancer. *Seminars in Cancer Biology* **2018**, *50*, 90–100.
- (31) Konarev, P. V.; Volkov, V. V.; Sokolova, A. V.; Koch, M. H.; Svergun, D. I. PRIMUS: a Windows PC-based system for small-angle scattering data analysis. *Journal of applied crystallography* **2003**, *36* (5), 1277–1282.
- (32) Svergun, D. Determination of the regularization parameter in indirect-transform methods using perceptual criteria. *Journal of applied crystallography* **1992**, *25* (4), 495–503.
- (33) Svergun, D. I.; Petoukhov, M. V.; Koch, M. H. Determination of domain structure of proteins from X-ray solution scattering. *Biophysical journal* **2001**, *80* (6), 2946–2953.
- (34) Kozin, M. B.; Svergun, D. I. Automated matching of high-and low-resolution structural models. *Journal of applied crystallography* **2001**, *34* (1), 33–41.
- (35) Volkov, V. V.; Svergun, D. I. Uniqueness of ab initio shape determination in small-angle scattering. *Journal of applied crystallography* **2003**, *36* (3), 860–864.
- (36) Kumar, A.; Ghosh, B.; Poswal, H.; Pandey, K.; Hosur, M.; Dwivedi, A.; Makde, R. D.; Sharma, S. M. Protein crystallography beamline (PX-BL21) at Indus-2 synchrotron. *Journal of Synchrotron Radiation* **2016**, *23* (2), 629–634.
- (37) Battye, T. G. G.; Kontogiannis, L.; Johnson, O.; Powell, H. R.; Leslie, A. G. iMOSFLM: a new graphical interface for diffraction-image processing with MOSFLM. *Acta Crystallographica Section D: Biological Crystallography* **2011**, *67* (4), 271–281.
- (38) Evans, P. Scaling and assessment of data quality. *Acta Crystallographica Section D: Biological Crystallography* **2006**, *62* (1), 72–82.
- (39) Collaborative Computational Project, Number 4 The CCP4 suite: programs for protein crystallography. *Acta Crystallographica Section D, Biological Crystallography* **1994**, *50* (5), 760–763.
- (40) Winn, M. D.; Ballard, C. C.; Cowtan, K. D.; Dodson, E. J.; Emsley, P.; Evans, P. R.; Keegan, R. M.; Krissinel, E. B.; Leslie, A. G.; McCoy, A. Overview of the CCP4 suite and current developments. *Acta Crystallographica Section D: Biological Crystallography* **2011**, *67* (4), 235–242.
- (41) McCoy, A. J.; Grosse-Kunstleve, R. W.; Adams, P. D.; Winn, M. D.; Storoni, L. C.; Read, R. J. Phaser crystallographic software. *Journal of applied crystallography* **2007**, *40* (4), 658–674.
- (42) Emsley, P.; Cowtan, K. Coot: model-building tools for molecular graphics. *Acta crystallographica section D: biological crystallography* **2004**, *60* (12), 2126–2132.
- (43) Murshudov, G. N.; Skubák, P.; Lebedev, A. A.; Pannu, N. S.; Steiner, R. A.; Nicholls, R. A.; Winn, M. D.; Long, F.; Vagin, A. A. REFMAC5 for the refinement of macromolecular crystal structures. *Acta Crystallographica Section D: Biological Crystallography* **2011**, *67* (4), 355–367.
- (44) Case, D.; Ben-Shalom, I.; Brozell, S.; Cerutti, D.; Cheatham, T., III; Cruzeiro, V.; Darden, T.; Duke, R.; Ghoreishi, D.; Gilson, M. AMBER 2018; University of California, San Francisco, 2018.
- (45) Steinbrecher, T.; Latzer, J.; Case, D. Revised AMBER parameters for bioorganic phosphates. *J. Chem. Theory Comput.* **2012**, *8* (11), 4405–4412.
- (46) Lambrakos, S. G.; Boris, J.; Oran, E.; Chandrasekhar, I.; Nagumo, M. A modified shake algorithm for maintaining rigid bonds in molecular dynamics simulations of large molecules. *J. Comput. Phys.* **1989**, *85* (2), 473–486.
- (47) Humphrey, W.; Dalke, A.; Schulten, K. VMD: visual molecular dynamics. *J. Mol. Graphics* **1996**, *14* (1), 33–38.